Clays and Clay Minerals, Vol. 43, No. 5, 515–524, 1995.

LEAD-210 DERIVED SEDIMENTATION RATES FROM A NORTH LOUISIANA PAPER-MILL EFFLUENT RESERVOIR

WILLIAM N. PIZZOLATO[1] AND RENÉ A. DE HON[2]

[1] U.S. Army Corps of Engineers, Waterways Experiment Station
Geotechnical Laboratory, CEWES-GG-YH, 3909 Halls Ferry Road
Vicksburg, Mississippi 39180

[2] Department of Geosciences, Northeast Louisiana University
Monroe, Louisiana 71209

Abstract—Lower Wham Brake is a cypress, rim-swamp artificially enclosed in 1950 as a 22 km^2 industrial reservoir by the International Paper Company (IPC)-Bastrop Mill, for regulating downstream water quality. Sediment cores were examined by XRD to differentiate paper-mill effluent deposition from the underlying detrital sediments and by ^{210}Pb decay spectroscopy to determine sediment accretion rates.

Anatase and kaolin from the IPC paper-mill effluent delineated a well-defined, anthropic, silty-clay, A horizon above a clay, 2Ag horizon. Anatase concentrations were no greater than 1.7% in the A horizon and was absent in the underlying 2Ag1 horizon. Kaolin deposition was significantly correlated to the A horizon by an average increase of 84% above the kaolinite detrital background. Pyrite was detected in the A horizon as a transformation mineral following sulfur reduction of the paper-mill effluent.

Five of the six sediment cores showed an inflection in the excess ^{210}Pb activity profile consistent with a present-day reduction in sediment supply. The average modern sedimentation rate was 0.05 cm yr^{-1}. Average sedimentation observed during historic accretion was 0.22 cm yr^{-1}, about 4.4 times greater than the modern rate of accretion. Reduction in sediment accretion can be attributed to upstream levees completed in 1934 and loss of organic accumulation following the 1950 reservoir impoundment. However, radiometric dating could not precisely correlate the geochronology of kaolin/anatase introduction due to complex oxidation/reduction cycles concurrent with the modern accretion regime.

Key Words—Anatase, Applied sedimentation, Kaolin, Lead-210, Paper-mill effluent, Pyrite, Wetland degradation.

INTRODUCTION

Numerous sedimentation studies have correlated excess ^{210}Pb deposition with a variety of procedures including radioisotope, palynological, elemental analysis, and natural sediment horizons in various environments (Wise 1980, Oldfield and Appleby 1984, Kearney *et al* 1985). Orson *et al* (1990) used excess ^{210}Pb activity profiles in conjunction with pollen, ^{137}Cs, ^{14}C analyses, and sediment flux rates to determine historic rates of sediment accumulation in a Delaware River tidal freshwater marsh. No other similar study has investigated a fresh-water, paludaul, industrial reservoir using radiometric decay analysis in conjunction with the identification of a paper-mill effluent mineral horizon.

This study uses a combination of analytical techniques (x-ray diffraction (XRD) and radiochemical spectroscopy) with soil core descriptions to quantify mineralogy and sedimentation. The data presented in this study is an interpretation of the depositional environment from Wham Brake Reservoir (Figure 1), operated and owned by International Paper Company (IPC), Bastrop, Louisiana. The applied sedimentation interpreted from excess ^{210}Pb activity profiles correlates anthropic mineral (anatase and kaolin) deposition and syngenetic (pyrite) mineralization from paper-mill effluent. Characterization of the sedimentation process within this paper-mill reservoir should be useful for providing a baseline estimate of the rate of burial for suspended particulate matter, such as hydrophobic dioxins.

Lead-210 is a naturally occurring radioisotope of the ^{238}U daughter decay series, which results from the intermediate decay of ^{226}Ra ($t_{1/2}$ = 1622 yr) to the noble gas, ^{222}Rn ($t_{1/2}$ = 3.83 d), by alpha disintegration (Goldberg 1963). Diffusing into the atmosphere at a constant flux, ^{222}Rn attaches to aerosols that return to the earth as precipitation or dry deposition. This atmospheric addition of ^{210}Pb is in excess of the amount supplied by the *in situ* decay of ^{226}Ra. Background or supported ^{210}Pb is assumed to be in equilibrium with the decay of ^{226}Ra without the negligible loss of radionuclides preceding ^{210}Pb. Lead-210 is highly particle reactive and is readily scavenged by organic matter and clay-size particles, but under anoxic conditions, ^{210}Pb can be released back to the water column (Benoit 1988).

Lead-210 ($t_{1/2}$ = 22.3 yr) is frequently used as a geochronometer in dating sediments up to 200 years before present (bp) (Oldfield and Appleby 1984). The assumption used in ^{210}Pb chronological interpretation is that upon burial, the radionuclide is immobile in sediments (Krishnaswami *et al* 1971). Caution is advised when interpreting excess ^{210}Pb activity profiles for es-

tablishing a geochronology in reducing environments. Studies by Koide *et al* (1973) and Benoit and Hemond (1990, 1991) showed that ^{210}Pb can be redistributed in lake sediments with seasonally anoxic bottom waters by pore water diffusion. The redistribution of ^{210}Pb in some fresh-water environments may be of sufficient magnitude to cause significant dating errors when mobilized ^{210}Pb is reprecipitated on younger sediments.

Wham Brake is a series of artificially enclosed, shallow, cypress lakes within the boundaries of southwest Morehouse and northeast Ouachita Parishes of northeast Louisiana. The basin is a rim-swamp situated on a Holocene meander-belt floodplain once occupied by an abandoned Arkansas River course 8500 to 6200 years bp (Saucier 1967). The reservoir is surrounded by a levee/spillway complex on three sides and flanked by Pleistocene terrace escarpments on the west and northwest. Drainage into Wham Brake is through Little Bayou Boeuf, which receives IPC mill effluent and Bastrop municipal wastewater discharges via Staulkinghead Creek. Impoundments are held for most of the year until the winter-spring season when the downstream dissolved oxygen and discharge are at sufficient levels to permit releases of Wham Brake via the Bayou Lafourche Diversion Canal (IPC, 1992, personal communication).

The southern extension of the reservoir complex enclosing the study area (hereafter to be known as Lower Wham Brake) has an approximate area of 22.0 km^2. Soils underlying the reservoir belong to the Yorktown series, a very-fine, montmorillonitic, nonacid, thermic, Typic Fluvaquents (Reynolds *et al* 1985). This series possesses hydric soil characteristics (National Technical Committee 1991) with a gleyed A horizon displaying a matrix chroma of two or less when mottles are present or a matrix chroma of one or less without mottles (Soil Survey Staff 1992, Vepraskas 1992). The Yorktown soils of Morehouse Parish are very poorly drained, very poorly permeable soils on level slopes, and these soils are taxadjuncts to the Yorktown series due to the lower pH than the nonacid (pH > 5.0) defined range for this series (Reynolds *et al* 1985). Wetland vegetation grows sporadically on the spoil banks of the dredge channels and along the levee banks. Virtually all cypress trees within the reservoir are dead and fishing is prohibited due to chemical contamination.

Natural runoff constitutes the majority of inflow into Wham Brake normally during the winter-spring months. For most of the year, the principal inflow into Wham Brake Reservoir is from sources other than natural runoff. Negating the Bastrop municipal wastewater and IPC mill effluent, Little Bayou Boeuf would hardly be a perennial stream during the summer months. The drainage area for Wham Brake Reservoir (including Staulkinghead Creek) is approximately 144.3 km^2 and has an average annual runoff rate of 1.7 m^3/s (61 CFS)

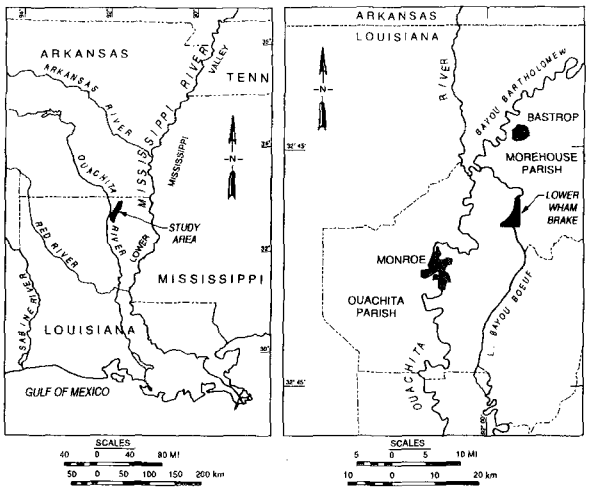

Figure 1. Location of Wham Brake Study area in the Lower Mississippi Valley situated along the boundary between Ouachita and Morehouse Parishes, Louisiana and to the south of the town of Bastrop.

calculated from surrounding river gaging stations (IPC, 1992, personal communication). No gaging data are available for Little Bayou Boeuf, but the estimated runoff potential entering Wham Brake Reservoir for the years 1988 through 1990 averaged 3.3 m^3/s (116 CFS). The 7-day 10-year low discharge (7Q10) to Wham Brake Reservoir is approximately 0.02 m^3/s (0.74 CFS). The average Bastrop municipal wastewater discharge of 0.05 m^3/s (1.7 CFS) plus the IPC mill effluent discharge of 1.2 m^3/s (41.6 CFS) contributes 98% of the 7Q10 inflow to Wham Brake Reservoir (IPC, 1992, personal communication).

METHODS

Field collection and handling

Ten (7.6 cm diameter) cores were obtained for particle-size determinations, clay analysis, and soil descriptions, of which six cores were analyzed for excess ^{210}Pb activity. Water depths are consistently uniform outside of the main channel of Little Bayou Boeuf, ranging from 0.8 to 1.2 m when the reservoir is at gage (spillway) elevations between 20.1 and 20.5 m.

Extracted cores were generally less than 30 cm in length and were sectioned every 1 to 2 cm over the entire core length. Bulk samples were dried at 105°C and gravimetric porosity measurements were calculated for each depth interval. For each depth interval, the sides were scraped to remove cross-contamination. Samples were disaggregated after removing woody debris (>2 cm), and splits were taken for XRD and ^{210}Pb analyses.

XRD analysis

Forty-eight samples from ten cores in the sediment profile were separated by particle size by gravity set-

https://doi.org/10.1346/CCMN.1995.0430501 Published online by Cambridge University Press

tling and centrifugation as outlined by Jackson (1969) and Folk (1974). Samples were dispersed in a 2.55g L^{-1} sodium hexametaphosphate solution and agitated for ten minutes. The sediment suspensions were dried at 105°C, and classified on a soil textural diagram. Organic content of the bulk sediment was measured by loss on ignition (LOI) at 450°C for four hours.

Soil clay suspensions (0.6 to 2.0 μm equivalent spherical diameter, esd) were centrifuged on glass slides as outlined by Spoljaric (1971, 1972). Clay minerals were scanned by XRD using Ni-filtered, CuKα radiation generated at 40 kV and 35 mA. The scanning speed was 0.02°2θ s^{-1} from 2 to 40°2θ with an automatic theta compensating slit of 0.2 mm. The relative weight percentage of clay minerals was determined by the analytical method of Schultz (1964).

Anatase was also examined by XRD as another mineral stratigraphic marker. Splits from the clay suspensions (<2.0 μm esd) were oven-dried, crushed, and heat-treated at 550°C for one hour. The 002*l* kaolinite reflection was removed by dehydroxylation from the shoulder of the principal anatase 101 hkl reflection before the sample was scanned as a randomly oriented powder. Peak area measurements (24.3–26.3°2θ) were compared for reagent grade anatase, for untreated samples, and for a known weight percent of anatase added to the untreated sample.

^{210}Pb methods and materials

Total ^{210}Pb activity is inferred radiochemically by assaying the α activity of ^{210}Po. Due to the weak β activity (0.018 MeV) during decay of ^{210}Pb to ^{210}Bi ($t_{1/2}$ = 5 d), direct measurement of ^{210}Pb is difficult (Robbins 1978). Bismuth-210 undergoes an energetic (1.17 MeV) β decay to ^{210}Po ($t_{1/2}$ = 138 d). Polonium-210 decays via a highly energetic (5.305 MeV) α activity to stable ^{206}Pb (Benoit 1988). Polonium-210 activity is utilized for two reasons: 1) the radioisotope is easily measured by low detection alpha spectroscopy, and 2) both ^{210}Bi and ^{210}Po have short half-lives following ^{210}Pb decay relative to the short time the sediment remains in the environment before collection. In a closed system where sediments are buried, ^{210}Po is present at the same concentration as ^{210}Pb, assuming that both isotopes remain under secular equilibrium (Benoit and Hemond 1990).

Bulk sediment samples were prepared following the procedure outlined by Flynn (1968) except ^{209}Po was substituted for ^{208}Po as the yield indicator. The ^{210}Po and ^{209}Po activities (Table 1, Core WB-1) were counted using a Canberra® alpha spectrometer. The activities are calculated as:

$$A(^{210}Pb) = \left(\frac{N_{210}s^{-1}}{N_{209}s^{-1}}\right)\left(\frac{A(^{209}Po)}{\text{g sediment}}\right) \quad (1)$$

where N_{209} and N_{210} are alpha counts of the polonium isotopes; $A(^{209}Po)$ = 20.06 dpm ml^{-1} (disintegrations per minute per milliliter) is the ^{209}Po decay activity coefficient. Statistical counting errors (Table 1) were calculated for excess ^{210}Pb data point by the equation:

$$A(^{210}Pb_{xs}) = (1/N_{209} + 1/N_{210})^{1/2}\, A(^{210}Po_{xs}) \quad (2)$$

The equation was further modified by taking into account the average of the lowest three supported ^{210}Pb activities found in the bottom of the core as a 1 sigma % error:

$$\Sigma = \{A(^{210}Pb_{xs})^2 + A(^{210}Pb_{sup})^2\}^{1/2} \quad (3)$$

and represents the statistical counting error shown as the horizontal bars (Table 1, Gaboury Benoit 1992, personal communication).

The sample depths in the sediment column are corrected for sediment consolidation by normalizing the depth profile to the lowest porosity value observed near the bottom of the core (Nittrouer *et al* 1979). This correction is necessary to prevent overestimating the sediment accretion rate.

The consolidation equation is:

$$L_2 = \left(\frac{(\rho_w C_{s1} L_1)}{(\rho_s C_{w1}) + (\rho_w C_{s1})}\right)\left(\frac{(C_{w2}\rho_w)}{(\rho_w C_{s2})} + 1\right) \quad (4)$$

where C_{s1} is the sediment mass before consolidation; C_{w1} is the water content before consolidation; L_1 is the unit length before consolidation; C_{s2} is the sediment mass after consolidation; C_{w2} is the water content after consolidation; ρ_s is the particle density of the sediments (2.60 g cm^{-3}); ρ_w is the pore water density (1.01 g cm^{-3}); and L_2 is the consolidated unit length (Brent A. McKee 1992, personal communication). Each consolidated interval is a representative midpoint of the depth in the core half the distance to the next sample. Mass sedimentation (Table 1) is calculated by the equation (Nittrouer *et al* 1984):

$$\omega = (1 - C_{w2})\rho_s\left(-\frac{\lambda}{m}\right) \quad (5)$$

where, ω is the mass sedimentation (g cm^{-2} yr^{-1}) rate determined from ^{210}Pb decay constant λ (0.03114 yr^{-1}). When the excess ^{210}Pb activity is plotted on a logarithmic scale against a corrected linear mass depth, the resulting profile determined by regression analysis gives a slope m of reliable accuracy (Shukla and Joshi 1989).

The sample depth (Table 1) midpoint uncertainty (MU) between successive intervals is represented as:

$$MU = (K_2 + K_1)/2 \pm (K_2 - K_1)/2 \quad (6)$$

where K_1 is the total mass depth from the surface to the top of the interval of interest, and K_2 is the total mass depth including the interval of interest (Gaboury Benoit 1992 personal communication).

The sedimentation (cm yr^{-1}) rate S is determined by:

https://doi.org/10.1346/CCMN.1995.0430501 Published online by Cambridge University Press

Table 1. Calculation of total Lead-210 activities from polonium radioisotopes, mass depth midpoints, and counting error departures for core WB-1.

Interval (cm)	Porosity (%)	Mass depth thickness (g/cm^2)	K1 (g/cm^2)	K2 (g/cm^2)	Midpoint uncertainty (g/cm^2)	Cumulative mass depth (g/cm^2)	Po-209 counts (cts/s)	Po-210 counts (cts/s)	Total Pb activity (dpm/g)	Total Pb error (%)
0–2	95.6	0.229	0.000	0.229	0.114	0.114	4871	5163	4.252	10.0
2–4	94.2	0.530	0.229	0.759	0.265	0.494	3811	3692	3.887	10.5
4–6	90.5	1.024	0.759	1.784	0.512	1.271	3277	1776	2.174	8.4
6–8	86.4	1.732	1.784	3.515	0.866	2.649	4469	2046	1.837	7.3
8–10	81.8	2.678	3.515	6.193	1.339	4.854	2346	845	1.445	7.9
10–11	79.7	3.206	6.193	9.399	1.603	7.796	2172	747	1.380	7.9
11–12	77.6	3.788	9.399	13.187	1.894	11.293	4067	1411	1.392	6.9
12–13	75.5	4.425	13.187	17.612	2.213	15.400	3622	1302	1.442	7.1
13–14	74.8	5.080	17.612	22.693	2.540	20.153	4245	1536	1.452	6.9
14–15	75.0	5.730	22.693	28.423	2.865	25.558	4105	1475	1.442	6.9
15–16	75.8	6.360	28.423	34.783	3.180	31.603	3600	1142	1.273	6.9
16–17	71.8	7.093	34.783	41.876	3.546	38.329	4014	1317	1.316	6.8
17–18	69.0	7.899	41.876	49.774	3.949	45.825	3252	1090	1.345	7.1
18–19	67.3	8.749	49.774	58.523	4.375	54.149	3174	952	1.203	7.0
19–20	64.8	9.664	58.523	68.188	4.832	63.356	2695	855	1.273	7.3
20–21	63.2	10.621	68.188	78.809	5.311	73.498	3629	1123	1.242	6.8
21–22	61.4	11.809	78.809	90.433	5.812	84.621	3051	893	1.174	7.0
22–23	61.5	12.626	90.433	103.059	6.313	96.746	1444	435	1.209	8.5
23–24	61.7	13.621	103.059	131.326	6.811	109.870	1532	372	0.974	7.8
24–25	60.5	14.646	116.680	131.326	7.323	124.003	1702	424	0.999	7.6
25–27	60.5	16.700	131.326	148.026	8.350	139.676	2079	533	1.030	7.3

$$S = -\frac{\lambda}{m} \quad (7)$$

which is the vertical sediment accretion when the excess ^{210}Pb activity is plotted on a logarithmic scale against a corrected linear consolidated (compacted) depth; the resulting profile determined by regression analysis yields the slope m.

The method for interpreting the sedimentation rates found in Lower Wham Brake uses the CIC (constant initial concentration of excess ^{210}Pb) model of Krishnaswamy *et al* (1971). The sedimentation rate using the CIC model is based on the assumptions that: 1) the ^{210}Pb depositional flux and sediment supply remains constant, 2) there is no migration of the associated radionuclides after burial, and 3) the supported activity of ^{210}Pb from the *in situ* decay of ^{226}Ra is independent of depth (Robbins and Edgington 1975). The CIC model employs measurements of sediment porosity to correct for compaction that can significantly overestimate the sedimentation rate S (Robbins and Edgington 1975, Robbins 1978, Shukla and Joshi 1989). The relationship of Krishnaswamy *et al* (1971) plots excess ^{210}Pb activity to depth z as:

$$A(z) = \frac{P}{\rho s} e^{-\lambda(z/S)} \quad (8)$$

where P is the depositional flux for excess ^{210}Pb after burial below the sediment-water interface, $e^{-\lambda}$ is the exponential of the natural logarithm 2 divided by the ^{210}Pb decay constant per year ($e^{-\lambda} = \ln 2/22.3\ yr^{-1} = 3.114 \times 10^{-2}\ yr^{-1}$). At depth and below any region of physical mixing or bioturbation, temporal variations in P or S generally yield a straight line from the log-linear profile.

RESULTS

Sediment characteristics

Lower Wham Brake sediment texture ranges downcore from silty clay in the A horizon to clay in the 2Ag horizons. The LOI organic content ranges from a high of 6.37% in the A horizon to a low of 1.45% in the 2Ag2 horizon. The A horizon has an average 12 cm thickness of low-shear strength sediment containing little recognizable organic debris and exudes the distinctive odor of hydrogen sulfide. This horizon is characterized by a soil matrix of low chroma (≤ 2) which upon air exposure ranges from very dark gray (N /3) to dark olive gray (5Y 3/2) to dark grayish brown (10YR 3/1). Redoximorphic features are few and increase to common with depth, faint to distinct in contrast, less than 15 mm in diameter, and represent soft concentrations of organic stains of dark gray color (5Y 4/1).

Below the A horizon, an irregular, abrupt boundary exists. The 2Ag horizon exhibits considerably greater plasticity and stickiness than the overlying A horizon. The gleyed sediment is characterized by dark brown (10YR 3/2) to very dark gray (10YR 3/1) to black (10YR 2.5/1) matrix colors. Redoximorphic features are common and decrease to few with depth, faint to distinct in contrast, and occur as soft, diffuse, masses between 5 to 15 mm in diameter. Redoximorphic colors include dark gray to gray (10YR 4/1, 10YR 5/1 or

5Y 5/1), which are redox depletions of Fe and Mn within the soil matrix (Vepraskas 1992). The soil structure is massive. Little change in chroma or hue in the matrix color was noted.

Soil reaction (dry) of bulk soil samples measured from the A/2Ag1 horizons after 60 days ranged from extremely acid to moderately acid (pH 4.1 to 5.8), while the 2Ag2 horizon ranged from very strongly acid to neutral (pH 4.9 to 7.2). Approximately two months is the maximum time portions of the reservoir are subaerially exposed following drawdown. The zone of saturation for Yorktown soil series is maintained during the months October through August ranging from average depth of +1.5 to −0.15 m (National Technical Committee 1991), but when the reservoir is artificially drained, only the A and 2Ag1 horizons would be exposed to the oximorphic process.

XRD results

A diffraction pattern (Figure 2) representative of Lower Wham Brake sediments illustrates the predominantly illite-kaolinite material mixed with a poorly crystalline expandable component. Illite and quartz increase with depth at the expense of kaolinite. Illite, vermiculite, smectite, and mixed-layer clays contribute more than half to three-quarters of the bulk clay mineralogy of clay-size fraction of the 2Ag horizons (Pizzolato 1994). Pyrite is absent a few centimeters below the sediment-water interface but increases with depth toward the bottom of the A horizon. Pyrite disappears a few centimeters below the A/2Ag1 interface and was not detected throughout the 2Ag2 horizon. Nine randomly oriented samples yielded detectable amounts of anatase ranging from 0.4 to 1.7% detected wholly within the A horizon (Pizzolato 1994).

Kaolin was introduced into Wham Brake around 1940 from the deposition of the paper-mill effluent (IPC 1992, personal communication). Kaolinite content (Figure 3) shows two distinct groups between the A and 2Ag horizons. The regression trend shows decreasing kaolinite content with depth ($n = 40$, $r = 0.737$, $P < 0.001$). Twenty-three oriented samples from the A horizon have a range of kaolinite between 22.5 to 61.2% with a mean of 45.4%. Seventeen oriented samples from the 2Ag horizons have a range of kaolinite from 21.3 to 32.0% with a mean of 24.7%. The A horizon contains 84% more kaolinite than the amount measured in the 2Ag horizons. The relative percentage of kaolinite in the coarse-clay fraction of soils surrounding the Wham Brake watershed ranges from 10 to 40% (Reynolds *et al* 1985).

^{210}Pb activity profiles

Excess ^{210}Pb activity profiles illustrate the distribution of the radioisotope upon burial presented as two categories of sedimentation. The first category, mass sedimentation (ω) is presented as a logarithmic plot of excess ^{210}Pb activity versus a plot of linear mass depth. The ^{210}Pb activity is delineated by horizontal error bars representing the statistical counting error and vertical range bars correspond to the mass depth midpoint uncertainty. As a comparison each core has two corresponding mass depth profiles showing: 1) the soil kaolinite and porosity percentage within designated soil horizons (Figure 4a), and 2) the sedimentation rates (g cm^{-2} yr^{-1}) for each corresponding activity regression (Figure 4b).

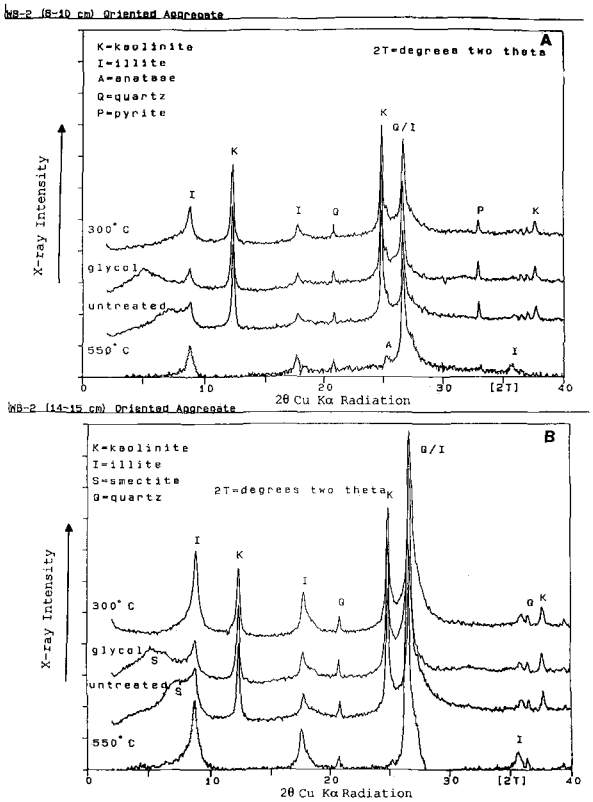

Figure 2. XRD patterns for oriented clay aggregates A. Sample WB-2 (8–10 cm) containing 46.9% kaolinite in a pyrite-enriched A horizon. B. Sample WB-2 (14–15 cm) containing 24.6% in a pyrite-free 2Ag1 horizon. Depths are uncorrected for compaction. All diffraction patterns recorded at the same scale.

Excess ^{210}Pb activity, seen as a vertical profile of uniform activity at shallow mass depth is interpreted as a mixing region and is omitted from the sedimentation rate calculations. Core WB-7 is the best example of this disturbance. Excess ^{210}Pb activity is uniformly distributed by sediment resuspension or bioturbation in a mixing zone between 0–25 g cm^{-2}. Comparison with soil porosity in WB-7 shows increasing porosity with depth in the A horizon corresponding with a similar trend of slightly higher excess ^{210}Pb activity. Other mixing regions (WB-2, WB-10) are shallow regions between 0–5 g cm^{-2} or is absent (WB-3).

https://doi.org/10.1346/CCMN.1995.0430501 Published online by Cambridge University Press

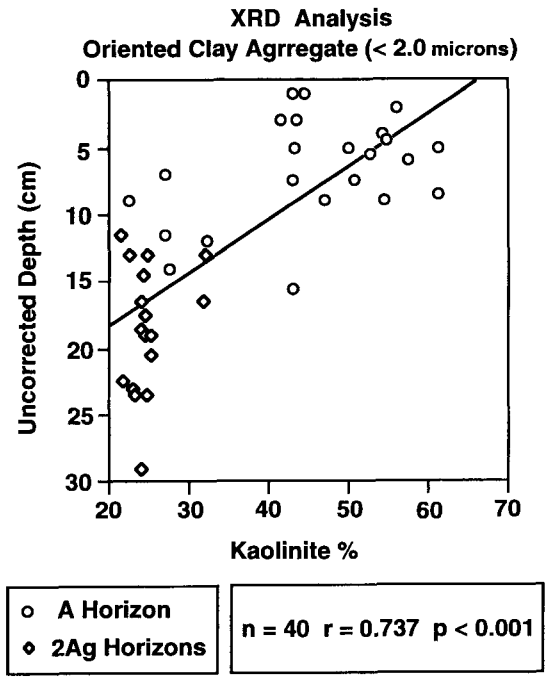

Figure 3. Kaolinite weight percentage for selected sediment horizons of ten cores showing two distinct groups relating effluent kaolin deposition to the A horizon and detrital kaolinite to the 2Ag horizons.

Excess ^{210}Pb activity, located between 5–25 g cm^{-2}, extends downcore with a low slope for all cores except WB-7. Excess ^{210}Pb activity is similar to the trend with porosity, however, there is an abrupt decrease in the kaolinite content at the A/2Ag1 boundary. Apparently the paper-mill effluent kaolin is not being reworked by physical mixing or bioturbation into the 2Ag1 horizon and the slope for the region of modern accretion is monotonic. Mass sedimentation observed for the region of modern accretion ranged from 0.038 to 0.356 g cm^2 (r^2 = 0.950 to 0.992).

An inflection in the slope of excess ^{210}Pb activity occurs between the region of modern and historic accretion. At the lower end of the modern accretion slope, excess ^{210}Pb activity is lower than the corresponding deeper samples of the historic accretion slope for cores WB-2, WB-3, and WB-10 (Figure 4b). The historic accretion slope becomes steeper and initial excess ^{210}Pb activity is higher than the corresponding samples above the inflection point. This evidence lends support to the CIC model that changing inputs of sediment supply and/or migration of excess ^{210}Pb are probable causes for two different sedimentation rates, one operative on each side of the inflection point in the profile. Mass sedimentation observed for the region of historic accretion ranged from 0.338 to 3.380 g cm^2 (r^2 = 0.636 to 0.934). Thus, the sedimentation rate ω for present-day modern accretion represents a 7.1 fold reduction over the rate observed in the region of historic accretion.

The second category of sedimentation plots excess ^{210}Pb activity on a logarithm scale against a linear scale of consolidated (corrected) depth (Figure 5). Using linear regression, an average vertical accretion rate (cm yr^{-1}) is calculated for the sedimentation rate S. Using the CIC model, the inflection point between two activity slopes again may be interpreted as a change in the rate of sediment supply (Krishnaswamy *et al* 1971). Vertical accretion rates observed in the region of modern accretion ranged from 0.029 to 0.076 cm yr^{-1} (r^2 = 0.916 to 0.975) whereas the rate for historic accretion was from 0.069 to 0.323 cm yr^{-1} (r^2 = 0.655 to 0.988). Therefore, the region of modern accretion represents a 4.4 fold decrease in the S rate over the historic accretion.

DISCUSSION

Corroborating ^{210}Pb dating with the introduction of paper-mill effluent minerals in this reservoir proved difficult and was not attempted. However, we argue that the apparent reduction in sedimentation rates in Lower Wham Brake Reservoir is the result of two possible mechanisms, excess ^{210}Pb diffusive redistribution and physical reduction of sediments.

Benoit and Hemond (1990, 1991) present evidence that postdepositional mobility of ^{210}Pb in stratified, anoxic waters occurs by pore water diffusion and rapid horizontal mixing/dilution in shallow sediments. Upon oxidation, iron precipitation is a particulate suitable for rescavenging ^{210}Pb. Frequent oxidation/reduction cycles, acidic soil pH, and S-enriched effluent are probable factors in the redox transformation of iron minerals to insoluble sulfides in this Lower Wham Brake reservoir. Lead-210 is exchangeable by pH < 6.5 to a greater extent than can be achieved by a reduction in the redox potential (Gambrell *et al* 1976).

The A horizon contains detectable levels of FeS_2 to a depth of 12 cm (uncorrected depth), but is absent from the underlying 2Ag horizons. Reduction of SO_4^{2-} to S^{2-} occurs when the redox potential is less than −150 mV and at a pH between 6.5 to 8.5 (Connell and Patrick 1968). Ferric iron is reduced to ferrous iron at higher redox potentials between +300 mV and +100 mV within a pH range between 5 to 7 (Gotoh and Patrick 1974). As a result, reduced iron is present before sulfide is formed. Hydrogen sulfide does not accumulate in fresh-water marsh soils high in iron (Whitcomb *et al* 1989). Under oxygen-limiting conditions, ferrous materials react with excess H_2S to form iron monosulfides (FeS) which in the presence of the elemental S catalyst forms FeS_2 (Berner 1970). Water-soluble ferrous Fe decreases as Eh increases from anaerobic to aerobic conditions; however, FeS_2 oxidation and sulfuric acid formation create large increases in soluble Fe. When conditions change from aerobic to

https://doi.org/10.1346/CCMN.1995.0430501 Published online by Cambridge University Press

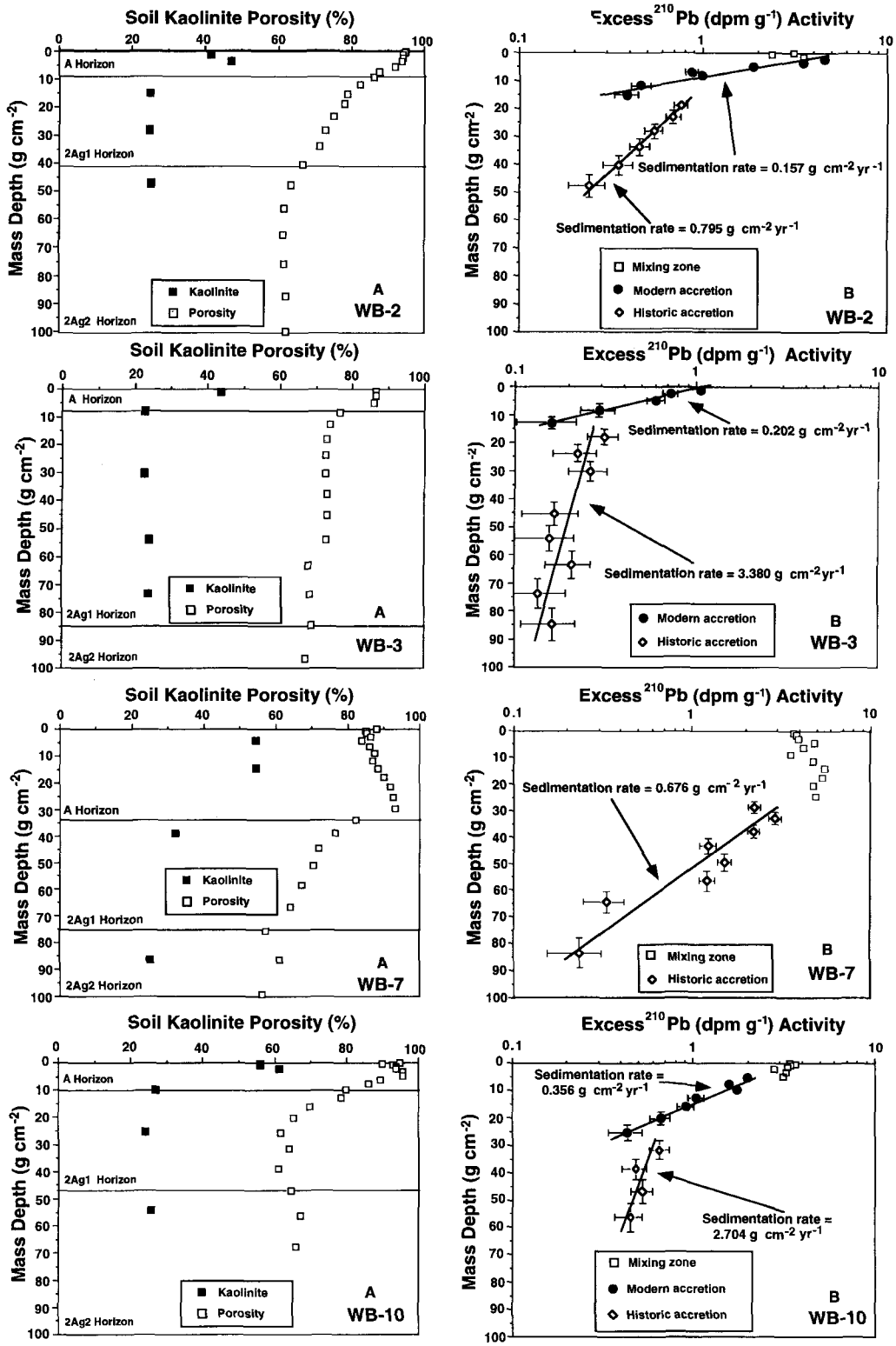

Figure 4. A. Percent porosity and kaolinite for cores WB-2, WB-3, WB-7, and WB-10 in selected soil horizons. B. Excess ^{210}Pb activity (dpm g^{-1}, disintegration per minute per gram of dry sediment) profiles for cores WB-2, WB-3, WB-7, and WB-10. Mass sedimentation (ω) rates are shown. Horizontal error bars represent the statistical counting error and vertical range bars correspond to the mass depth midpoint uncertainty.

https://doi.org/10.1346/CCMN.1995.0430501 Published online by Cambridge University Press

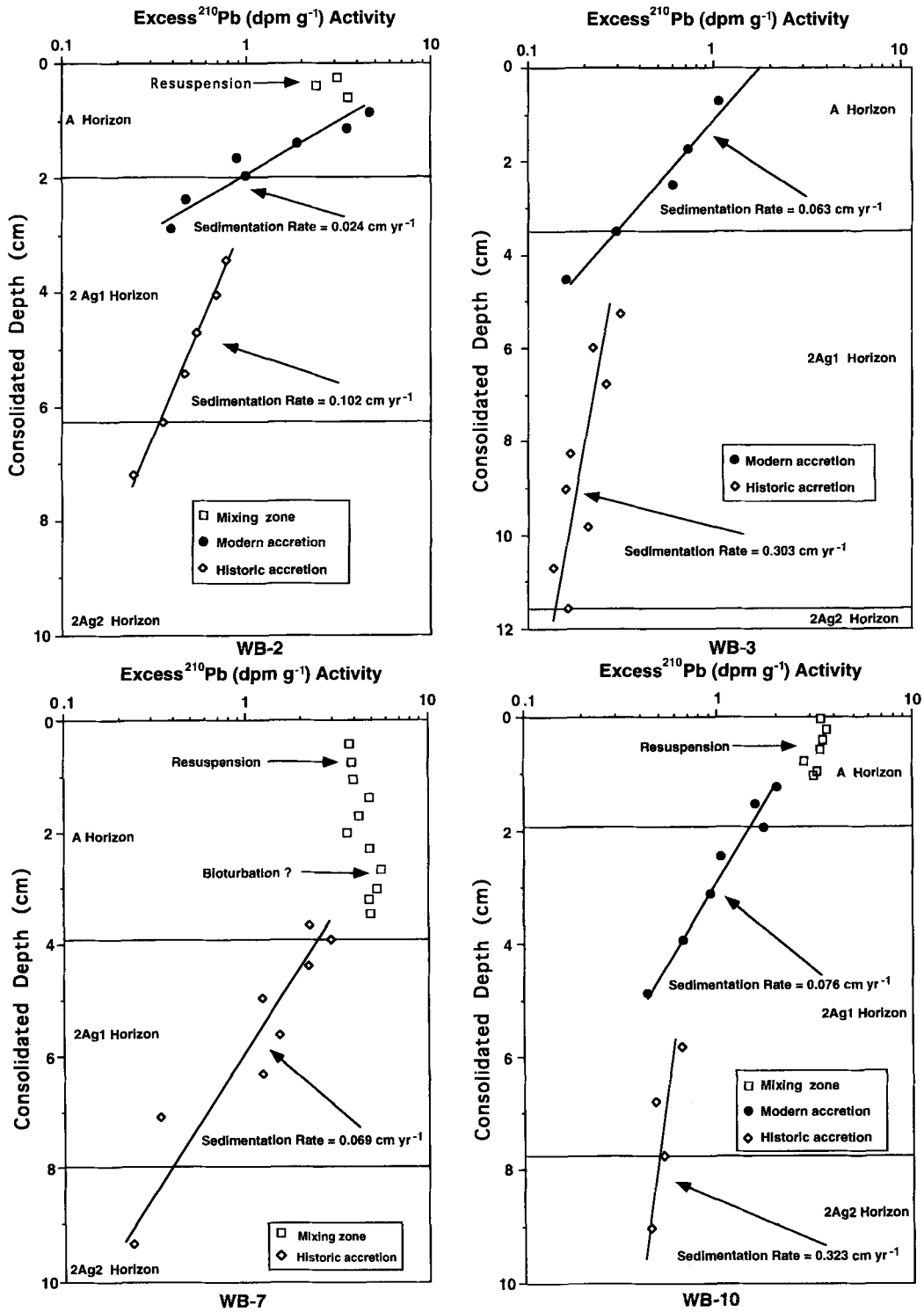

Figure 5. Sedimentation profile for cores WB-2, WB-3, WB-7, and WB-10 determined by excess ^{210}Pb activity and corrected for compaction within various soil horizons. Vertical accretion sedimentation (S) rates are shown.

https://doi.org/10.1346/CCMN.1995.0430501 Published online by Cambridge University Press

anaerobic conditions, Fe^{+2} increases until FeS precipitates as Eh decreases to −50 mV (Satawathananont *et al* 1991). While the process for the sulfate-sulfide cycling is not known, i.e., biological or inorganic mechanisms, the introduction of paper-mill effluent is the principal source of S entering Wham Brake Reservoir.

Below an uncorrected, average depth of 12 cm, within the 2Ag1 horizon, the absence of FeS_2 corresponds with a reduction of organic-matter content and H_2S generation. Thus, the limiting factor for pyritization in the mineral horizon most likely is a paucity of labile organic carbon available to anaerobic micro-organisms. FeS_2 oxidation occurs so slowly that soil buffering processes, such as diffusion, leaching, degassing, and jarosite formation can maintain the soil pH around 4.0 (Satawathananont *et al* 1991).

At the lower end of the modern accretion slope below the A/2Ag1 boundary, excess ^{210}Pb activity is lower than the initial activity of the region of historic accretion (Figures 4b and 5). The activity slope decreases montonically with depth toward the lower end of the inflection and is governed by the depth of the redox at which the radioisotope is remobilized. Below this inflection point, initial ^{210}Pb activity is higher than the position above and the slope of excess ^{210}Pb profile is steeper than before the diffusive flux.

Partial loss of ^{210}Pb activity indicates remobilization of ^{210}Pb by pore water diffusion and reprecipitation above the A/2Ag1 boundary. The activity between 5–25 g cm^{-2} (Figures 4b) is thought to be the most likely region for excess ^{210}Pb redistribution where pyrite is observed. The higher kaolin content of the A horizon provides partial evidence for excess ^{210}Pb redistribution by pore water diffusion, since sediment reworking would disperse the paper-mill effluent minerals into the 2Ag1 horizon and excess ^{210}Pb would appear as a vertical profile of uniform activity.

Benoit and Hemond (1991) developed an empirical model which evaluated evidence for the diffusive redistribution of ^{210}Pb in anoxic lake sediments. Porosity and sediment bulk density influence the pore water concentration gradient of ^{210}Pb; thus, ionic transport influences the apparent ^{210}Pb redistribution profile in reduced sediments. Their model indicated that the diffusive flux was greatest at 86% porosity, with 80% of this maximum value occurring between a range of 63 to 97%. This range typifies Lower Wham Brake sediments and illustrates the differences in the sediment horizons. Decaying roots and woody debris provide sufficient voids for enhancing secondary porosity in the upper mineral horizons. Excess ^{210}Pb activity from core WB-7 (Figure 4) increases slightly with depth and mirrors the porosity trend before reversing below the A/2Ag1 boundary.

While the exact mechanism for excess ^{210}Pb redistribution is not known because of the annual cycles of inundation and drawdown, physical reduction of the present-day sedimentation rate cannot be ruled out. Sulfur-enriched water as well as changes in the hydroperiod have been shown to stress a cypress swamp within one year (Richardson *et al* 1983). A reduction in the annual buildup of litter facilitates less organic accumulation that serves to trap inorganic sediments. Land use records reveal that backwater control levees, completed in 1934, restricted overflow drainage from Bayou Bartholomew entering the Little Bayou Boeuf drainage area (Corps of Engineers-Vicksburg District 1994, personal communication). A physical reduction of inorganic, suspended sediment is entirely plausible since the apparent time of the inflection between the modern and historic accretion is from 1895 to 1940. It is probable that the reduction of sedimentation rates was initiated prior to 1950 completion of Wham Brake Reservoir, but wetland degradation within the reservoir lessens the rate of organic accumulation.

CONCLUSIONS

Historic allochthonous accretion into Lower Wham Brake was found to be at a low level (0.22 cm yr^{-1}), and the modern sedimentation is believed to accreting at an even lower rate (0.05 cm yr^{-1}). The reduction in sedimentation rates appears reasonable where backwater control levees completed in 1934 have restricted overflow entering the reservoir's drainage basin. The lower rate of accretion today results from a lower inorganic sediment supply and the loss of organic accumulation attributed to wetland degradation by the reservoir inundation and H_2S toxicity. Due to the anoxic environment prevalent during most of the year and the periodic winter–spring reservoir drawdown, non-steady state conditions complicate an interpretation of the uppermost excess ^{210}Pb activity profile for establishing a reliable geochronology with the 1940 kaolin depositional horizon. Physical resuspension of sediments is evident by the nearly vertical mixing profile caused by wind-driven reservoir fetch. Below this sediment resuspension, the modern accretion region is thought to be an artifact of diffusive horizontal transport of excess ^{210}Pb activity under non-steady state conditions and its redistribution concurrent with FeS_2 precipitation. The paper-mill effluent deposition of anatase and kaolin is diagnostic of the A horizon and is not observed within the 2Ag horizons. The A horizon contains 84% more kaolin than the detrital kaolinite background and is negatively correlated with depth in the 2Ag horizons. The region of historic accretion has excess ^{210}Pb activity that is least affected by ionic diffusion and redistribution due to lower porosity and a low organic content. However, until a detailed analysis of the Wham Brake Reservoir redox system is undertaken, it can only be speculated whether or not remobilization of excess ^{210}Pb represents a strategy of diffusion and redistribution within the region of modern accretion during annual oxidation/reduction cycles. The data are suggestive, however, that reduction of the modern sedimentation rate in this constructed

wetland reservoir may be concurrent with biogeochemical and anthropic processes. These processes alter excess ^{210}Pb activity to the extent that correlation between the geochronology of this radioisotope and deposition of the paper-mill effluent anatase/kaolin horizon is suspect.

ACKNOWLEDGMENTS

This research was supported by grants provided by The Geological Society of America, The Clay Minerals Society, and International Paper Corporation. The authors gratefully acknowledge Dr. Brent McKee, Louisiana Universities Marine Consortium, for providing laboratory support in the ^{210}Pb analysis and to Dr. Gaboury Benoit, Yale University, for his helpful comments regarding the figures.

REFERENCES

Benoit, G. 1988. The biogeochemistry of ^{210}Pb and ^{210}Po in fresh waters and sediments: Ph.D. dissertation. Massachusetts Institute of Technology at Cambridge, 304 pp.

Benoit, G., and H. F. Hemond. 1990. ^{210}Pb and ^{210}Po remobilization from lake sediments in relation to iron and manganese cycling. *Environ. Sci. Technol.* **24**: 1224–1234.

Benoit, G., and H. F. Hemond. 1991. Evidence for diffusive redistribution of ^{210}Pb in lake sediments. *Geochim. Cosmochim. Acta* **55**: 1963–1975.

Berner, R. A. 1970. Sedimentary pyrite formation. *Am. J. Sci.* **268**: 1–23.

Connell, W. E., and W. H. Patrick Jr. 1968. Sulfate reduction in soil: Effects of redox potential and pH. *Science* **159**: 86–87.

Flynn, W. W. 1968. The determination of low levels of polonium-210 in environmental materials. *Anal. Chim. Acta* **43**: 221–227.

Folk, R. L. 1974. Petrology of Sedimentary Rocks. Austin, Texas: Hemphill Publishing Company, 184 pp.

Gambrell, R. P., R. A. Khalid, and W. H. Patrick Jr. 1976. Physiochemical parameters that regulate mobilization and immobilization of toxic heavy metals. In *Proceedings of the Specialty Conference on Dredging and its Environmental Effects.* American Society of Civil Engineers, New York, 418–434 pp.

Gotoh, S., and W. H. Patrick Jr. 1974. Transformation of iron in a waterlogged soil as influenced by redox potential and pH. *Soil Sci. Soc. Amer. Proc.* **38**: 66–71.

Goldberg, E. D. 1963. *Geochronology with ^{210}Pb in Radioactive Dating.* Vienna: International Atomic Energy Agency, 121–131.

Jackson, M. L. 1969. *Soil Chemical Analysis-Advanced Course.* M. L. Jackson ed. Madison, Wisconsin: 895 pp.

Koide M., K. W. Bruland, and E. D. Goldberg. 1973. Th-228/Th-232 and Pb-210 geochronologies in marine and lake sediments *Geochim. Cosmochim. Acta* **37**: 1171–1187.

Kearney, M. S., L. G. Ward, C. M. Cofta, G. R. Helz, and T. M. Church. 1985. Sedimentology, geochronology and trace metals in the Nanticoke and Choptank Rivers, Chesapeake Bay. In *Tech. Rep. No. 84.* College Park: University of Maryland, 94 pp.

Krishnaswamy, S., D. Lal, J. M. Martin, and M. Meybeck. 1971. Geochronology of lake sediments. *Earth Planet. Sci. Lett.* **11**: 407–414.

National Technical Committee for Hydric Soils 1991. *Hydric Soils of the United States,* 3rd ed. Washington, D.C.: USDA-Soil Conservation Service.

Nittrouer, C. A., R. W. Sternberg, R. Carpenter, and J. T. Bennet. 1979. The use of Pb-210 geochronology as a sedimentological tool: application to the Washington continental shelf. *Mar. Geol.* **31**: 297–316.

Nittrouer, C. A., D. J. DeMaster, B. A. McKee, N. H. Cutshall, and I. L. Larson. 1984. The effect of sediment mixing on Pb-210 accumulation rates for the Washington continental shelf. *Mar. Geol.* **54**: 210–221.

Oldfield, F., and P. G. Appleby. 1984. Empirical testing of 210Pb-dating models for lake sediments. In *Lake Sediments and Environmental History.* E. Y. Hayworth and J. W. G. Lund, eds. University of Minnesota Minneapolis: Press, 93–124.

Orson, R. A., R. L. Simpson, and R. E. Good. 1990. Rates of sediment accumulation in a tidal freshwater marsh. *J. of Sedimentary Petrology* **60** (6): 859–869.

Pizzolato, W. N. 1994. X-ray diffraction study of sediments from a paper-mill effluent reservoir, Ouachita and Morehouse Parishes, Louisiana. *The Compass,* **70**: 4.

Reynolds, E. F., E. T. Allen, T. L. May, and T. A. Weems. 1985. *Soil Survey of Morehouse Parish Louisiana:* Washington D.C.: USDA-Soil Conservation Service, 175 pp.

Richardson J., P. A. Straub, K. C. Ewel, and H. T. Odum. 1983. Sulfate-enriched water effects on a floodplain forest in Florida. *Envir. Management* **74**: 321–326.

Robbins, J. A. 1978. Geochemical and geophysical applications of radioactive lead. In *The Biogeochemistry of Lead in the Environment.* J. Nriagu, ed. Amsterdam: Elsevier, 284–393.

Robbins J. A., and D. N. Edgington. 1975. Determination of recent sedimentation rates in Lake Michigan using Pb-210 and Cs-137. *Geochim. Cosmochim. Acta* **39**: 285–304.

Satawathananont, S., W. H. Patrick Jr., and P. A. Moore Jr. 1991. Effect of controlled redox conditions on metal solubility in acid sulfate soils. *Plant and Soil* **133**: 281–290.

Saucier, R. 1967. Geological investigation of the Boeuf-Tensas Basin, Lower Mississippi Valley. Technical Report 3-757. Vicksburg: U.S. Army Corps of Engineer WES, 57 pp.

Schultz, L. G. 1964. Quantitative interpretation of mineralogical composition from x-ray and chemical data for the Pierre Shale: Professional Paper 391-C, U.S. Geological Survey, Washington D. C., 31 pp.

Shukla, B. S., and S. R. Joshi. 1989. An evaluation of the CIC model of ^{210}Pb dating of sediments. *Environ. Geol. Water Sci.* **14**(1): 73–76.

Soil Survey Staff 1992. Keys to Soil Taxonomy: 5th ed., SMSS Technical Monograph No. 19, Pocahontas Press, Blacksburg, Virginia, 541 pp.

Spoljaric, N. 1971. Quick preparation of slides of well-oriented clay minerals for x-ray diffraction analysis. *J. Sed. Petrol.* **41**: 589–590.

Spoljaric, N. 1972. Reply to Comment on 'Quick preparation of slides of well-oriented clay minerals for x-ray diffraction analysis'. *J. Sed. Petrol.* **42**: 249–250.

Vepraskas, M. J. 1992. Redoximorphic features for identifying aquic conditions. In *Tech. Bull. 301.* North Carolina State University at Raleigh, 33 pp.

Whitcomb, J. H., R. D. DeLaune, and W. H., Patrick Jr. 1989. Chemical oxidation of sulfide to elemental sulfur: Its possible role in marsh energy flow. *Mar. Geol.* **26**: 205–214.

Wise, S. M. 1980. Caesium-137 and Lead-210: a review of the techniques and some applications in geomorphology. In *Timescales in Geomorphology.* R. A. Cullingford, D. A. Davidson, and J. Lewin, eds. New York: John Wiley & Sons, 110–127.

(Received 15 April 1994; Accepted 15 January 1995; Ms. 2496).